$^3P_2$ argon would be quite large, since its structure is grossly similar to that of ground-state potassium, which has a polarizability of about 36×10^{-24} cm^3. Further, since the valence electron contributes the major amount to the polarizability, the polarizability ratio $\alpha_z(+1)/\alpha_z(+2)$ should be quite close to unity. (The valence electron is in an s state.)

The P configuration of the atom is due to the five p electrons of the incomplete M shell, whose contribution to the polarizability should therefore contain a strong anisotropy. However, since the contribution of the core to the total polarizability is small, the net anisotropy should also be small.

ACKNOWLEDGMENTS

We wish to thank Professor Arthur Salop for his continued interest, and for many useful discussions and suggestions during the course of the work. We also wish to thank Judah Levine for his assistance during the latter part of the experiment.

PHYSICAL REVIEW VOLUME 134, NUMBER 5A 1 JUNE 1964

Studies of the Mechanism of Electron-Ion Recombination. II

WILLIAM A. ROGERS* AND MANFRED A. BIONDI†
Westinghouse Research Laboratories, Pittsburgh, Pennsylvania
(Received 13 January 1964)

Microwave, optical spectrometric, and interferometric techniques have been used to investigate the nature of the electron-ion recombination process in low-pressure, pure helium afterglows at 300 and 77°K. To determine whether dissociative capture of electrons by helium molecular ions, i.e., $He_2^+ + e \rightarrow He^* + He + (KE)$, is the recombination reaction taking place, we have attempted to detect the kinetic energy of dissociation of the excited atoms produced in the recombination process by a study of the widths of the emitted afterglow lines. A model of the low-pressure helium afterglow which reasonably accounts for our electron density, line intensity, and linewidth observations involves principally the creation of He^+ ions and electrons by the collisions of pairs of helium metastable atoms, the three-body conversion of He^+ ions to He_2^+ ions, the ambipolar diffusion of He^+, He_2^+, and electrons, and the diffusion of helium metastable atoms to the walls. The $\lambda5876$ radiation (3^3D-2^3P transition) from the later part of the afterglow, when recombination of He_2^+ and electrons is expected to be the source of the excited atoms, exhibits a substantial broadening over the approximately thermal width observed during the discharge and in the early afterglow, when the radiation is expected to originate from electron impact excitation of helium atoms. It is concluded that the dissociative recombination process is the likely source of the observed afterglow line broadening.

I. INTRODUCTION

NUMEROUS experimental studies of the afterglows of pulsed microwave discharges[1–4] have shown that volume electron-ion recombination appears to be an important or dominating process in the removal of free electrons from ionized gases for several different gases. The principal technique in these experiments has involved the determination of spatially averaged electron densities during the afterglow by means of microwave probing techniques (see part I of this paper,[5] hereinafter referred to as I) and an analysis of the time dependence in terms of solutions of the equation of continuity for electrons subject to losses by recombination and diffusion. This analysis, as commonly employed, is outlined in Eqs. (3)–(6) of I.

In the rare gases neon and argon, it has been possible to obtain experimental data consistent with the recombination solution, $1/n_e=[1/n_e(0)]+\alpha t$, and thus to evaluate the recombination coefficient α with reasonable precision. In helium, however, due to the larger ratio of diffusion loss to recombination loss it has not been possible to obtain such a clear distinction. In addition, the helium measurements have been complicated by the fact that at pressures of only a few mm Hg the atomic spectra, which are presumably related to the recombination process, give way to molecular spectra of excited He_2. Thus, serious doubts have been cast on the validity of measurements of the recombination coefficient in helium by means of the afterglow time dependence studies.[6]

By means of a set of controlled mixture experiments in helium and argon, it has been shown (see I) that the large recombination coefficients observed in the pure gases do not appear under circumstances that inhibit

* Present address: Physics Department, Thiel College, Greenville, Pennsylvania.
† Physics Department, University of Pittsburgh, Pittsburgh, Pennsylvania.

[1] M. A. Biondi and S. C. Brown, Phys. Rev. **76**, 1697 (1949).
[2] R. B. Holt, J. M. Richardson, B. Howland, and B. T. McClure, Phys. Rev. **77**, 239 (1950).
[3] M. A. Biondi and T. Holstein, Phys. Rev. **82**, 962 (1951); M. A. Biondi, *ibid.* **83**, 1078 (1951).
[4] A. C. Faire and K. S. W. Champion, Phys. Rev. **113**, 1 (1959).
[5] M. A. Biondi, Phys. Rev. **129**, 1181 (1963).
[6] C. S. Leffel, M. N. Hirsch, and D. E. Kerr, Ann. Phys. (N. Y.) (to be published).

the formation of diatomic molecular ions, thus supporting the hypothesis of Bates[7] that the process under observation is the dissociative recombination of molecular ions with electrons in the reaction,

$$X_2^+ + e \rightarrow X^* + X + \text{kinetic energy}. \quad (1)$$

This naturally leads to the supposition that the same process is responsible for any large recombination loss occurring in moderate-pressure helium afterglows.

The purpose of the experiments reported in this paper has been (a) to establish definitely the presence or absence of the dissociative recombination process in pure helium afterglows at low pressures (2 mm Hg or less) by a technique which avoids the complexity and uncertainty of interpretation inherent in the microwave electron-density determinations under mixed diffusion and recombination conditions, and (b) to provide an estimate of the magnitude of the recombination coefficient, if possible. The principal new technique introduced is the interferometric measurement of the intensity profile of an optical emission line of the helium atomic spectrum.

The significance of this measurement can be understood by reference to Fig. 1 and to Eq. (1) and from the following considerations. The dissociative process can be efficient only if it is exothermic, i.e., the transition from the bound state A to the dissociated state B must be accompanied by the conversion of potential energy into kinetic energy in a significant amount. This converted energy is shown as the vertical scaled length E_D in the figure. The kinetic energy so produced is shared by the fragments which fly out from the dissociating system. In the case of a homonuclear diatomic molecule, this energy of dissociation E_D is shared equally by the two identical atoms. Also, in the case of helium, the relative energies of the molecular-ion ground state and the molecular and atomic states are such that one of the atoms will almost certainly be produced in an electronically excited state.

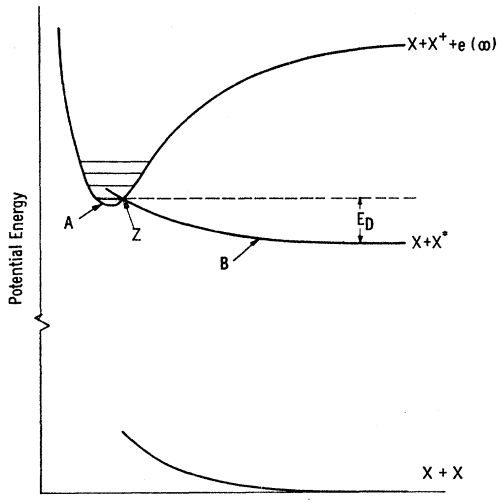

FIG. 1. Schematic representation of the interatomic potential curves of interest in the dissociative recombination of X_2^+ ions with electrons. The upper potential curve is that for a molecular ion and an electron at rest at infinity.

[7] D. R. Bates, Phys. Rev. **77**, 718 (1950); **78**, 492 (1950); **82**, 103 (1951).

If this excited atom is produced in a radiating state of sufficiently short lifetime, it can be expected to radiate some of its excitation energy before it has time either to lose its kinetic energy through collisions or to lose its excitation energy by resonant transfer to a slowly moving atom. If the atom does radiate before experiencing energy loss of either kind, the emitted photon will be shifted from its normal wavelength by the Doppler effect due to the atomic velocity. Since there is no preferred direction for dissociation, the velocities of the dissociating atoms will be randomly directed, and consequently, the observed effect will be a Doppler broadening of the atomic spectral line in excess of the broadening due to the temperature of the molecular ions by an amount corresponding to the kinetic energy $E_D/2$. The direct observation of such anomalous line broadening may be taken as positive evidence of the predominance of the dissociative recombination process in the production of the afterglow emission spectrum.

For this type of measurement helium has been chosen, rather than neon or argon, primarily because of the simplicity of its optical spectrum and the short lifetimes of some of the radiating states. Since the analysis involves considerable computation, a single line (λ5876, corresponding to the transition $3\,^3D$–$2\,^3P$) has been chosen for study.

The linewidth studies have been correlated with electron-density measurements and with time-resolved emission spectra. In addition to the recombination study itself, attention has been given to the early part of the afterglow preceding the "recombination" period which has been the subject of most previous investigations. An attempt has been made to formulate a complete model of the afterglow processes for a simple case.

II. EXPERIMENTAL SYSTEM

The complete experimental arrangement is shown diagrammatically in Fig. 2, except for the ultrahigh-vaccum gas handling system. The apparatus shown may be regarded as comprising three main units: microwave, spectrometer, and interferometer systems.

A. Microwave System

At the center of the figure is the microwave resonant cavity which encloses the discharge vessel and has hollow walls which may be filled with liquid nitrogen. A repeated, pulsed discharge is produced in the quartz discharge vessel by power from the magnetron. Following this pulse a very low power probing signal is applied from the klystron. Power reflected from the cavity

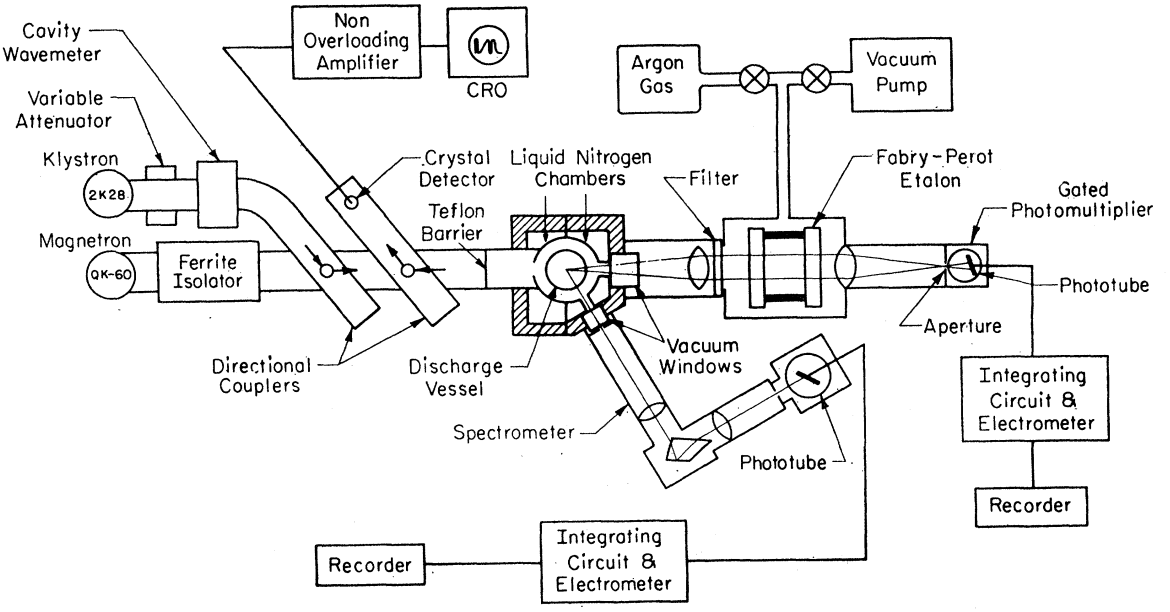

FIG. 2. Block diagram of the combined microwave, optical spectrometric, and optical interferometric systems used to study afterglows.

resonator is detected by the crystal detector and passed through an amplifier, which suppresses the strong magnetron pulse. The resulting signal is displayed on a synchronized oscilloscope.

B. Spectrometer System

A spectrometer port is provided by a narrow slit which tunnels through the double wall of the cavity resonator and an evacuated double glass window which tunnels through the foam insulation. The spectrometer has a synchronous prism table drive motor and an electronically gated multiplier phototube detector, whose output goes to an integrating filter, dc electrometer and synchronously driven strip chart recorder.

C. Interferometer System

A second small opening in the cavity wall, similar to the spectrometer port but circular in cross section, provides a port for the Fabry-Perot etalon. The etalon and detection system used here[8] is similar in principle to that used by Jacquinot and Dufour.[9] It is illustrated in more detail in Fig. 3.

The mechanical support and adjustment of the etalon plates (F) is provided by means of a conventional arrangement of invar spacers (G) and spring mounted compression pins (H) similar to those described in textbooks,[10] with modifications as required to permit operation through the walls of the evacuated housing (C). The photoelectric detection, integrating, and recording system is identical with that of the spectrometer system.

In use the etalon, Fig. 3, is placed so that the focal plane of the collimating lens (A) is near the center of the microwave cavity, i.e., in the middle of the discharge. The collimated beam passes from the lens through a glass color filter and multilayer interference filter (B),

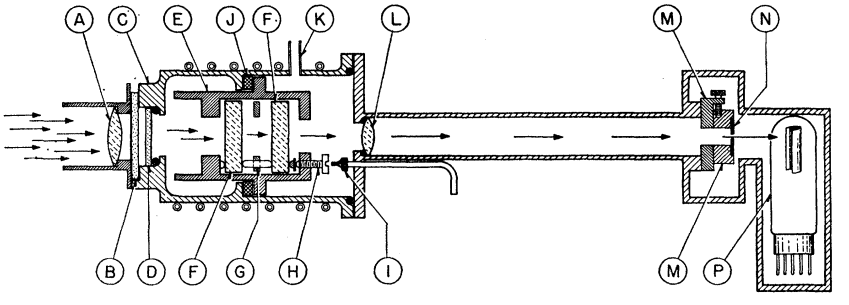

FIG. 3. Detailed cross section view of the photoelectric recording, Fabry-Perot interferometer. (See text for explanation.)

[8] M. A. Biondi, Rev. Sci. Instr. **27**, 36 (1956).
[9] P. Jacquinot and C. Dufour, J. Rech. Centre Natl. Rech. Sci. Lab., Bellevue (Paris) **6**, 91 (1949).
[10] See, for example, S. Tolansky, *High Resolution Spectroscopy* (Methuen and Co. Ltd., London, 1947).

through the optically clear vacuum window (D), the etalon plates (F), and the vacuum window and focusing lens (L). Here it is focused on an opaque disk (N) having in it a circular aperture of 0.051 cm diam which is centered on the interference pattern by the micrometer carriages (M) to within 0.001 cm. This aperture permits a very limited angular range of incident light, including a portion of the central spot of the interference pattern, to pass through to the photocathode.

From simple considerations of geometrical optics, one can calculate the luminous flux reaching the cathode of the multiplier phototube, assuming lossless optical elements. This calculation, together with rough measures of the absorption losses and the photocathode quantum efficiency, forms the basis for estimating absolute intensities in the afterglow.

The observed resolution of the etalon in practice is two parts in 10^6, in approximate agreement with the calculated value. The experimental value of resolution is based on measurements made (a) with a microwave discharge in argon containing a trace of isotopic Hg^{202} using the narrow Hg line at 5461 Å as a standard, and (b) on the assumption that the smallest attainable values of linewidth in helium are due solely to thermal Doppler broadening corresponding to the ambient temperature. The values deduced by the two different methods are in good agreement.

A wavelength scanning system with linear time base is provided for the etalon by continuously increasing the refractive index μ in the space between the etalon plates (see Fig. 2). This is achieved by first evacuating the interior of the sealed etalon housing with a vacuum pump to provide a starting point and then admitting gas through a preset needle valve connected to a source of argon at 200 atm pressure. The gas density in the etalon rises slowly from zero to slightly over one atmosphere, at which point further increase is interrupted by the opening of a safety valve. This system offers a uniform scanning rate over approximately 10 fringes. Since the synchronous motor drive on the recorder provides a linear time base for the chart paper, one obtains a linear presentation of intensity as a function of frequency (wavelength) within each interference order, thus giving us the desired line shapes directly.

D. Vacuum System

The gas is admitted to and removed from the quartz discharge vessel through a small bore tube which passes directly out of the cavity resonator through a close fitting hole at the upper end of the cavity axis. Through this tube the discharge vessel is connected to an ultrahigh-vacuum gas handling system[11] with a bakeable oil manometer[12] and a copper isolation trap.[13] The discharge vessel itself is isolated from the rest of the vacuum system by a liquid-nitrogen trap.

The helium gas for these experiments is prepared by distillation from the liquid into 1-*l* gas flasks. The flasks, connected to a special glass manifold which can be opened under liquid helium, are first prepared by being outgassed under ultrahigh-vacuum conditions; then the manifold is sealed off from the outgassing system under vacuum and transferred to the liquid-helium storage Dewar. After being filled by distillation from the liquid helium, the flasks are individually sealed off from the special manifold and sealed on to the operating vacuum system. After a bake-out of the whole system at 400°C overnight and the attainment of a vacuum level below 10^{-9} mm Hg, the sealed flask is opened. By comparison of visible spectra of our prepared pure helium with those of mass analyzed samples of reagent grade helium, it appears that in all gas samples used the impurity level has been less than one part in 10^7 and too small to detect.

III. EXPERIMENTAL AND ANALYTICAL PROCEDURES

A. Microwave Procedures

The average electron density as a function of time is determined by the technique of microwave reflection from the cavity resonator. This technique has been discussed in detail elsewhere and will not be reviewed here.[14]

In view of the high Q of the cavity resonator, it is not surprising that the growth of the discharge in response to the applied power should be quite complicated. The initial conditions of the afterglow seem to be most sensitive to the length of the power pulse and less sensitive to the repetition rate and power delivered from the magnetron. With the magnetron frequency set slightly above the resonant frequency of the cavity without discharge, the buildup of plasma density during the power pulse shifts the cavity resonance through the magnetron frequency to a higher frequency, at which point further increase in plasma density is prevented by the self-detuning of the cavity toward still higher frequencies. Observations have shown that in this system the discharge has passed through a maximum of light output and settled down to approximately the steady-state emission rate after about 40 μsec. Therefore, this value of the pulse duration has been set as an arbitrary standard for most of the experiments. Experience also showed that an afterglow period of about 2 msec is the least time in which the essential features of the time-dependent afterglow processes can be exhibited and, therefore, this has been used as the pulse repetition interval in most of the experiments.

B. Spectrometric Procedures

Using the high-speed optical spectrometer with gated multiplier phototube and recorder, comparisons have

[11] D. Alpert, J. Appl. Phys. **24**, 860 (1953); *Handbuch der Physik* (Springer-Verlag, Berlin, 1957), Vol. 12.
[12] M. A. Biondi, Rev. Sci. Instr. **24**, 989 (1953).
[13] D. Alpert, Rev. Sci. Instr. **24**, 1004 (1953).
[14] M. A. Biondi, Rev. Sci. Instr. **22**, 500 (1951).

been made of the intensities of several atomic lines at various times in the afterglow. The synchronous motor drives on the chart recorder and the spectrometer prism table provide a direct conversion of wavelength to chart length scale. By setting the electronic gate to any desired duration and to any desired onset delay relative to the end of the discharge, the afterglow spectrum has been recorded during each of several short periods (durations of 50–500 μsec) in the afterglow. Also, by stopping the prism table drive on the peak of any desired line and periodically changing the onset delay time of the gate, the time dependences of several individual lines have been traced. Attention was centered mainly on the diffuse series lines λ4472 and λ4922 ($4D$-$2P$) and λ5876 and λ6678 ($3D$-$2P$), although other lines of the sharp, principal, and diffuse series were also monitored.

Even at the low pressures of these experiments the spectrometer indicates the presence of some helium molecular-band intensity, which the etalon cannot resolve but shows as a "white" background to the desired atomic line emission. Therefore, the spectrometer has been used to determine the relative strengths of the bands that fall within the transmission range of the multilayer interference filter used with the etalon. The transmission of the interference filter together with its associated color filter was determined by comparing the spectrum of an incandescent lamp with and without interposition of the filter. Although the spectrometer does not resolve detailed structure of the bands and records atomic lines only as impulses whose shapes are fixed by the time constant of the electronic integrating circuit, the relative total strength (intensity integrated over wavelength range) of a band to a line is given by the ratio of the areas under the respective recorded contours. This information has been used to correct for the apparent line broadening which would result from the superposition of the band radiation on that of the line recorded by the etalon.

C. Linewidth Measurements with the Etalon

Several factors enter into the production of the observed atomic linewidth. Some of these factors are analytically separable; some must be treated as they appear. We now outline the analysis in terms of which the line broadening measurements are interpreted.

1. Single Component Line Shape due to Temperature and Dissociative Recombination

We assume that line broadening is entirely due to Doppler effects arising from temperature motion and from dissociation of the excited molecule. The kinetic-energy distribution of the diatomic ions is assumed to be Maxwellian at the gas temperature, so that it may be written

$$F_0(v)=(\beta/\pi)^{3/2}\exp(-\beta v^2), \tag{2}$$

where $\beta=M/kT$, M being the mass of a single helium atom. The problem is further simplified by assuming that all dissociations leading to a given excited atomic state originate in a single specific molecular configuration, and, therefore, release a definite total kinetic energy E_D which is shared equally by the two dissociating atoms. Thus, the speed of the excited atom relative to the center of mass of the diatomic ions is $v_1=(E_D/M)^{1/2}$. The direction taken by the atom is assumed to be randomly oriented with respect to the observer, so the distribution F_1 in velocity relative to the center of mass is simply a unit impulse function (δ function) of speed at v_1.

For the computation of Doppler shift we are interested only in the distribution in speed along the observer's line of sight (the z axis). For the thermal distribution we get by integration over the x-y plane

$$F_0(v_z)=(\beta/\pi)^{1/2}\exp(-\beta v_z^2), \tag{3}$$

while the integration of F_1 over the x-y plane yields

$$F_1(v_z)=1/2v_1 \tag{4}$$

for $-v_1\leqslant v_z\leqslant v_1$ and zero elsewhere.

The two distributions F_0 and F_1 are combined in the following way. For every v_z' at which atoms are repelled from the center of mass there is a complete Maxwellian distribution of velocities of the center of mass, giving rise to a group of atoms having a Maxwellian distribution centered on the value v_z'. That is, the number of atoms in the speed range dv_z' at v_z-v_z' is

$$dG=F_0(v_z-v_z')F_1(v_z')dv_z'. \tag{5}$$

The total resultant distribution in v_z is then obtained by integrating Eq. (5) over the entire range of v_z'. If we first substitute for v everywhere the corresponding Doppler wave number shift, $\tilde{\nu}=\tilde{\nu}_0 v/c$, and simplify notation by putting $a=(Mc^2/kT)^{1/2}/\nu_0$ and $b=(E_D/kT)^{1/2}$, we obtain as the resultant intensity contour (normalized to unit area)

$$G(\tilde{\nu})=(a/4b)[\mathrm{erf}(a\tilde{\nu}+b)-\mathrm{erf}(a\tilde{\nu}-b)]. \tag{6}$$

Analysis of $G(\tilde{\nu})$ shows that at the center of the line ($\tilde{\nu}$ much smaller than $\tilde{\nu}_1\equiv\tilde{\nu}_0 v_1/c$) the slope of $G(\tilde{\nu})$ equals the slope of $F_0(\tilde{\nu})$ multiplied by $\exp(-E_D/kT)$. If E_D is reasonably large compared to kT, the line shape $G(\tilde{\nu})$ will be tend to become very flat topped.

2. Instrumental Broadening of the Single Component Line

The fringe shape for monochromatic light of wave number $\tilde{\nu}$ passing through an etalon at normal incidence is given by Airy's formula[10]

$$I=T^2(1-R)^{-2}[1+K\sin^2(2\pi\mu t\tilde{\nu})]^{-1}, \tag{7}$$

where T is the transmission and R the reflectivity of the coatings on the etalon plates, μ is the index of refraction of the medium between the plates, t the plate

spacing, and $K=4R/(1-R)^2$. For present purposes we will omit the intensity reduction factor $T^2(1-R)^{-2}$ and write for the normalized etalon transmission function,

$$H(f)=(1+K\sin^2\pi f)^{-1}, \tag{8}$$

in which $f=2\mu t\tilde{\nu}$. The quantity f is the interference order number; it is used here as a dimensionless frequency variable measured in units of the free spectral range of the etalon. This is a simple scale change, which does not alter the form of G, Eq. (6), and provides a convenient unit for discussion of the etalon measurements.

The line shape resulting from the transmission of the line $G(f)$ through the etalon is obtained by considering the line as the superposition of fringes of all the monochromatic elements whose integral over frequency constitutes $G(f)$. Thus, if the etalon is set or "tuned" for a frequency f (i.e., the interference order is integral for f), then light at frequency f' produces a fringe intensity contribution of $G(f')H(f-f')df'$. The total resultant intensity transmitted at a given etalon setting is then

$$\phi(f)=\int_0^\infty G(f')H(f-f')df'. \tag{9}$$

This integral requires numerical computation. It has been computed at intervals of $f=0.01$ for several values of T and E_D, initially by manual tabulation and then more extensively by the computer facility of the Mathematics Department of the Westinghouse Research Laboratories. From the results so obtained, it was evident that no simple procedure would satisfactorily separate the instrumental contribution from the actual line broadening. For this reason the computed over-all profiles are compared directly with the observed total linewidths.

3. *Choice of the λ5876 Line and the Shape of the Triplet Line in the Etalon*

Although the singlet lines offer the obvious advantage of simplicity in their lack of fine structure, the λ5876 ($3\,^3D-2\,^3P$) line was selected because it has the shortest lifetime among all the visible transitions ($\tau_{\text{rad}}=1.34\times10^{-8}$ sec), is well isolated from neighboring lines, is known to be a bright line in low-pressure afterglows, and is in a wavelength region suited to available photoelectric tubes. Moreover, its terminal state, $2\,^3P$, is itself a radiating state and, therefore, not sufficiently populated to cause any spurious broadening by self-absorption. The high radiative transition rate of nearly 10^8 sec^{-1} was initially considered necessary to assure a high probability of radiation prior to excitation transfer or kinetic energy loss by collisions, which have been estimated to occur at a rate of the order of 10^8 per second at a pressure of one mm Hg. Thus, measurements of line shapes have been carried out at pressures of a few mm Hg or less.

An analysis of the structure of the λ5876 line had been made by Brochard *et al.*[15] using an etalon and a helium source cooled in liquid helium. Their results have been adopted as a basis for the construction of the expected line shapes. In our experiments it is not possible to separate each of the six components of the line because of temperature broadening. The etalon-free spectral range has been chosen to make the one separable component appear as a satellite one and one-half orders removed from the main peak composed of the other five. The fringe contributions of all six have been added graphically over the range of interest in the main peak, and resulting widths at half-intensity have been measured from the composite graph for a variety of parameter values. The half-widths of these lines have been compared with actually observed half-widths to determine E_D.

4. *Spurious Line Broadening Effects*

In addition to the temperature and dissociative recombination line broadening effects, there are two principal spurious effects which may lead to an apparent broadening of the observed lines. These are (a) the presence of molecular band radiation in the light reaching the photocathode, and (b) the effect of electrical integrating networks between the phototube and the electrometer.

Any molecular band radiation which passes through the interference filter and the etalon may be assumed to consist of numerous rotational transition lines, a fact which is corroborated by the shapes of the molecular bands as recorded through the spectrometer. These rotation lines are spaced nonuniformly in frequency and irrationally with the etalon-free spectral range. Consequently, they overlap each other in a random fashion and form what may be regarded as "white" light. To compare the effect of band radiation with that of an isolated atomic line we make the simplifying assumption that the etalon transmission function $H(f)$ is periodic in f with unit period, is unity over a range f_e equal to the etalon half-width, and zero in the remainder of each unit range; that the atomic line intensity $G(f)$ is a constant A over a range f_a equal to the half-width of the line and zero elsewhere, f_a being larger than f_e but less than unity; and that the molecular band intensity is a constant B over a frequency range f_b which is much greater than unity and zero elsewhere. With these very simple line shapes it can be readily shown that the etalon reduces the ratio of total band radiation to line radiation by the factor f_a. Checks on this procedure by graphical area measurements on the carefully computed etalon-Doppler lines show that the simple theory is always conservative in that it overestimates the molecular background by about 10–30%. The effect of a white background on atomic line half-width measurements is to displace the apparent zero intensity reference of the line downward, causing the half-width

[15] J. Brochard *et al.*, J. Phys. Rad. **13**, 433 (1952).

to be measured too low on the line profile, thereby giving too large a value for the half-width. A correction for this effect has been made which is accurate for narrow lines and/or small "white" backgrounds and which overestimates the spurious broadening for wider lines and/or larger "white" backgrounds. Thus, the deduced linewidths in the presence of molecular light background are smaller than the actual widths.

The electrical integrating circuits necessary to suppress noise and to convert the time-gated sample signals into dc signals for amplification and recording place a limit on the speed with which the line profile may be scanned. In practice, if the circuits are characterized by a response time constant τ and the line profile is traced between half-intensity points in a time Δt, care is taken to assure that $\Delta t \gtrsim 5\tau$ for the narrowest line in a set of measurements, leading to a distortion of the recorded profile which increases the apparent line breadth by less than 2%. The error in measured width for broader lines, which take even longer to trace, is even smaller.

IV. MODEL OF THE AFTERGLOW

The variations of the measured electron densities, spectral intensities, and line shapes during the afterglow are sufficiently complicated that it is of considerable help to have in mind the relevant atomic-collision processes which contribute to their behavior. The following model of the afterglow is consistent with previous researches on helium[16–18] and with the observations obtained in the present studies.

At the low pressures ($\sim$1 mm Hg) and moderate container size (fundamental diffusion length, $\Lambda_1 = 0.735$ cm) used in these afterglow studies, the principal loss of the electrons, ions, and metastable atoms is by diffusion to the container walls. In addition, there is substantial production of electrons and atomic ions by collisions of pairs of metastable atoms,[19]

$$\mathrm{He}^M + \mathrm{He}^M \rightarrow \mathrm{He}^+ + e + \mathrm{He}. \quad (10)$$

Since the excitation energy of the metastable state of the helium atom is $\sim$20 eV and the ionization potential $\sim$25 eV, the electrons produced by this reaction have $\sim$15 eV kinetic energy. As will be discussed more fully later, it is to be expected that before this excess kinetic energy is completely dissipated by elastic collisions, there is a substantial probability that these electrons will collide with metastable atoms, raising them to higher, radiating states, i.e.,

$$\mathrm{He}^M + e(\mathrm{fast}) \rightarrow \mathrm{He}^* + e(\mathrm{slow}). \quad (11)$$

The atomic ions produced in the ionizing reaction, Eq. (10), are converted to molecular ions in three-body collisions,[17]

$$\mathrm{He}^+ + 2\mathrm{He} \rightarrow \mathrm{He}_2^+ + \mathrm{He}. \quad (12)$$

While the major loss of molecular ions is by diffusion to the walls, dissociative recombination between molecular ions and electrons is expected to produce radiating atomic excited states according to the reaction

$$\mathrm{He}_2^+ + e \rightarrow \mathrm{He}^* + \mathrm{He}. \quad (13)$$

If we neglect small terms in the equations governing the production and loss of the atomic ions and the molecular ions, we obtain the following approximate relationships:

$$\partial n_1/\partial t \simeq D_{a1}\nabla^2 n_1 - K_c n^2 n_1 + \beta_i n_m^2 \quad (14)$$

and

$$\partial n_2/\partial t \simeq D_{a2}\nabla^2 n_2 + K_c n^2 n_1, \quad (15)$$

where D_{a1} and D_{a2} are the ambipolar diffusion coefficients of the atomic and molecular ions of densities n_1 and n_2, respectively, n is the neutral atom density, n_m the metastable concentration, K_c the three-body conversion coefficient for reaction (12), and β_i is the two-body ionizing coefficient for metastable-metastable collisions, Eq. (10). It is assumed that the above equations apply to thermal energy particles, since the electron- and ion-energy decay times are short ($\lesssim 10$ μsec) compared to the time scale of the measurements.

Since the molecular-ion concentration remains small compared to the atomic-ion density throughout these low-pressure afterglows, we may take the electron density, $n_e \simeq n_1$. Also, at low pressures (<1 mm Hg) the metastable atoms decay principally by diffusion to the walls; thus, the third term on the right of Eq. (14) may be approximated by $\beta_i n_m^2(0) \exp(-2\nu_m t)$, where ν_m is the diffusion frequency of the metastables. From the published values[16–18] of the atomic ion, molecular ion, and metastable atom diffusion coefficients, of K_c and β_i (see Table I), and assuming a metastable atom concentration sufficient to produce the observed maximum value for the electron density in the afterglow, i.e., $n_m(0) \sim 10^{12}$ cm^{-3}, one can calculate the afterglow behavior of the atomic ions, electrons, and molecular ions. The results of a model afterglow calculation at a pressure of 0.54 mm Hg and $T = 300$°K are shown in Fig. 4. Starting from a very small number of electrons

TABLE I. Coefficients used in the afterglow analysis (for references, see text).

		He^+	He_2^+	He^M ($2\,^3S$)
Diffusion, Dp	300°K	540	1015	520
(cm^2/sec)-(mm Hg)	77°K	173	230	130
Recombination, α (cm^3/sec)		$<10^{-10}$	1×10^{-8}	...
Ionization, β_i (cm^3/sec)		...	...	1×10^{-9}
Conversion, K_c (cm^6/sec)		6×10^{-32}	...	...

[16] M. A. Biondi and S. C. Brown, Phys. Rev. **75**, 1700 (1949).
[17] A. V. Phelps and S. C. Brown, Phys. Rev. **86**, 102 (1952).
[18] A. V. Phelps and J. Molnar, Phys. Rev. **89**, 1202 (1953); A. V. Phelps, *ibid.* **99**, 1307 (1955).
[19] M. A. Biondi, Phys. Rev. **88**, 660 (1952). Contrary to the conclusion of H. Myers, Phys. Rev. **130**, 1639 (1963), available experimental evidence (Refs. 17–19) strongly supports the conclusion that metastable-metastable ionizing collisions lead to the production of *atomic*, rather than molecular, helium ions.

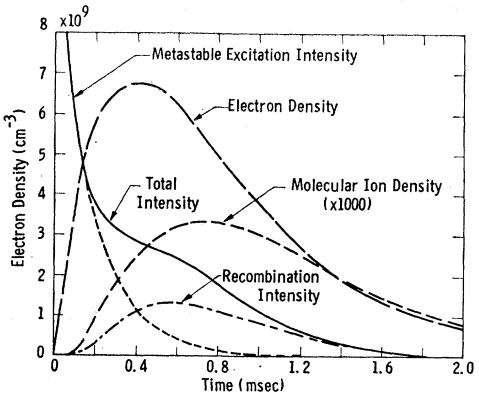

FIG. 4. Calculated behavior of various quantities in a helium afterglow at 300°K and a gas pressure of 0.54 mm Hg based on the model of the afterglow described in the text.

and atomic ions at the beginning of the afterglow, metastable-metastable ionizing collisions cause an increase in n_e and n_1. As the metastable density decreases, leading to a smaller ionization rate, the diffusion to the walls and conversion of atomic ions leads to the final decay of n_1 and n_e. Meanwhile, the molecular-ion density, which also started essentially from zero at the beginning of the afterglow, increases as a result of atomic ion conversion, reaching a considerably smaller maximum value than the electrons somewhat later in the afterglow.

One may account for the intensity variation of the afterglow radiation, as follows; in the early afterglow when metastable atoms are plentiful and molecular ions are absent the radiation should be the result of the production of fast electrons by metastable-metastable collisions which then excite other metastables to radiating states. Thus, the radiation produced by this process should decay at *three* times the metastable atom-decay rate.

Considering the electron's loss of kinetic energy at elastic collisions, it can be shown that approximately 6×10^3 collisions are required to reduce the electron's initial energy from $\sim$15 eV to the threshold value, $\sim$3 eV, for exciting $2\,^3S$ metastable atoms to the observed radiating states (e.g., $3\,^3D$). For the inferred initial metastable density of $\sim10^{12}$ cm^{-3}, the observed early radiation intensity can be accounted for, provided that the average cross section for excitation of the metastable state to a radiating state over the electron energy range from 3–15 eV is comparable to the cross section for scattering of electrons by normal atoms,[20] i.e., $\sim4\times10^{-16}$ cm^2. Although there are no direct measurements of electron impact excitation of metastable states, such a cross section does not seem unreasonable, since it is substantially less than the theoretical maximum value[21] for such a process. The predicted shape of the early afterglow radiation (metastable excitation intensity) is indicated in Fig. 4.

In the late afterglow, when the molecular ions have reached an appreciable concentration and the metastable atoms have diffused away, the radiation should be the result of excited states produced by dissociative recombination, reaction (13). The intensity of this radiation should, therefore, be roughly equal to $(\alpha n_e n_2)$, where α is the dissociative recombination coefficient, on the assumption that recombination predominantly produces the desired state either directly or by cascading from higher states. The recombination radiation intensity curve of Fig. 4 was predicted from the computed electron density and molecular-ion density curves and an assumed recombination coefficient of 1×10^{-8} cm^3/sec.[22] The total predicted intensity is then the sum of the metastable excitation and recombination intensities. The absolute intensities measured in the late afterglow are consistent with this model and the assumed recombination coefficient. However, the difficulties of the absolute intensity determinations are such that the values may be in error by up to a factor of 3.

It should be noted that, with the aforementioned model of the afterglow, the radiation resulting from metastable excitation by electron impact in the early afterglow should exhibit a thermal spectral linewidth. By contrast, the late afterglow radiation, which is assumed to result from the dissociative recombination process, should exhibit a broadened line shape.

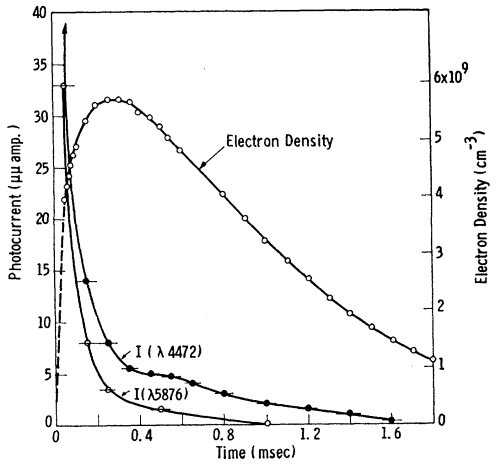

FIG. 5. Observed behavior of the electron density and the intensities of two lines emitted from a helium afterglow at 300°K and $p=0.54$ mm Hg. The line λ5876 corresponds to the $3\,^3D$–$2\,^3P$ transition; λ4472 to $4\,^3D$–$2\,^3P$.

[20] R. B. Brode, Rev. Mod. Phys. **5**, 257 (1933).

[21] H. S. W. Massey and E. H. S. Burhop, *Electronic and Ionic Impact Phenomena* (Clarendon Press, Oxford, 1952), p. 144.

[22] This value was used as an approximation of the results of C. L. Chen, C. C. Leiby, and L. Goldstein, Phys. Rev. **121**, 1391 (1961), who are the only investigators who achieved recombination control in their afterglow.

V. RESULTS AND DISCUSSION

The observations which led to the construction of the afterglow model discussed in the previous section suggested a natural subdivision of the afterglow into an early and a late period, based on the line intensity and linewidth variations. In Figs. 5 and 6 are shown the variations of n_e and of the intensities of λ5876 and λ4472 observed during afterglows at $T=300°K$ and 0.54 and 2.05 mm Hg pressure, respectively. It will be seen that the observations at 0.54 mm Hg reproduce qualitatively the predictions of the model shown in Fig. 4, in that the electron density reaches a maximum value at ~300 μsec in the afterglow and the intensity of λ4472 exhibits a slight hump at ~500 μsec. No comparisons with the 2.05 mm Hg data (Fig. 6) are made, since the simplifying assumptions used in the model calculation at 0.54 mm Hg pressure are no longer valid at the higher pressure.

On the basis of the proposed afterglow model one should expect significant changes in the character of the radiation emitted in the early and in the late afterglow. It is noted that in the early afterglow the relative intensities of the various lines emitted are quite similar to those observed during the discharge. In both cases the excited states are presumed to be produced principally by electron impact excitation of lower excited states (ground state or metastable states). From the observed intensities in the early afterglow, one deduces a population of excited states which decreases monotonically with increasing principal quantum number, n. (Lines from upper states $n=3$, 4, 5, 6 were observed.) By contrast, in the late afterglow a change in spectral distribution is noted, the relative population of the states of higher quantum numbers, e.g., $n=5$, increasing markedly in comparison to the early afterglow values. As will be seen in the later discussion, such a behavior is consistent with dissociative recombination into higher excited states.

A principal effort of the present investigation lay in the determinations of the widths of the λ5876 line during the discharge and at various times in the afterglow in order to test the dissociative recombination hypothesis. As discussed in Sec. IIIC, the measured linewidths include contributions from fine structure, Doppler broadening, and instrumental broadening. The results of the line broadening measurements are, therefore, presented in terms of the observed total linewidths, determined at the half-maximum intensity points and expressed as fractions f of the free spectral range of the etalon, $\Delta\tilde{\nu}_{fsr}=(2\mu t)^{-1}=0.667$ cm^{-1}. The "temperature" of excited atoms required to yield the Doppler broadening contribution is then determined from the line-shape calculations as described in Sec. III C.

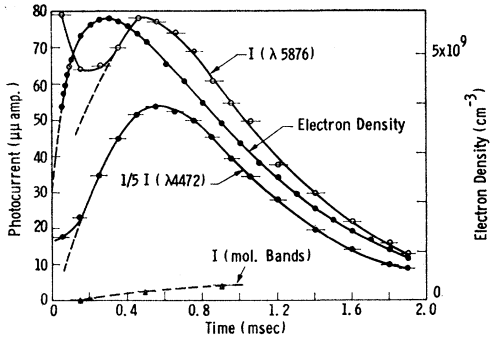

FIG. 6. Observed behavior of the electron density, two line intensities and the molecular band intensities in a helium afterglow at 300°K and $p=2.05$ mm Hg.

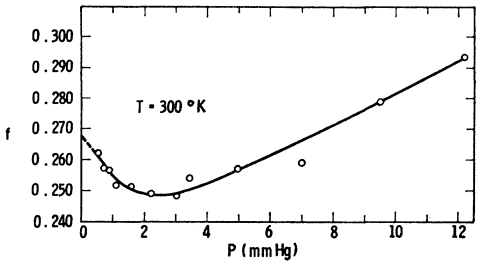

FIG. 7. Observed linewidth (including instrumental width) during the pulsed discharge in helium at 300°K. The linewidths are expressed as fractions f of the free spectral range of the Fabry–Perot etalon, $\Delta\tilde{\nu}_{fsr}=0.667$ cm^{-1}. The minimum width at ~3 mm Hg corresponds to the computed width for an excited atom temperature of ~300°K.

The observed width of the λ5876 line during the *discharge* in helium for various gas pressures is shown in Fig. 7. The minimum width observed at ~3 mm Hg corresponds to the linewidth calculated for an excited atom temperature of ~300°K. The increase in width at >3 mm Hg is the result of the appearance of some molecular light and pressure broadening effects. The increase in linewidth with decreasing pressure below 2 mm Hg can be shown to result from radiation of the excited atoms before they lose their recoil kinetic energy gained at the inelastic impact of the electrons having more than 23 eV kinetic energy which create the excited states. The linewidth data extrapolated to zero pressure are consistent with the expected recoil energy of ~0.004 eV, and the fact that this additional broadening does not disappear until ~3 mm Hg pressure suggests that excitation transfer to slow atoms and loss of kinetic energy by collisions of the excited atoms with normal atoms are slow enough to permit observation of line broadening due to dissociative recombination at pressures ≲2 mm Hg.[23]

The observed λ5876 linewidths in the afterglow, as well as during the discharge, are shown for several gas

[23] An alternative possibility is that narrowing of the discharge line may be due to a change in mode of production of excited states with change of gas pressure. If metastable $2\,^3S$ atoms reach a very large density $>10^{13}$ cm^{-3} as the pressure increases, then impact excitation to the $3\,^3D$ state by ~3 eV electrons will produce the observed intensity of λ5876 and the atom recoil energy will be too small to appreciably add to the thermal linewidth.

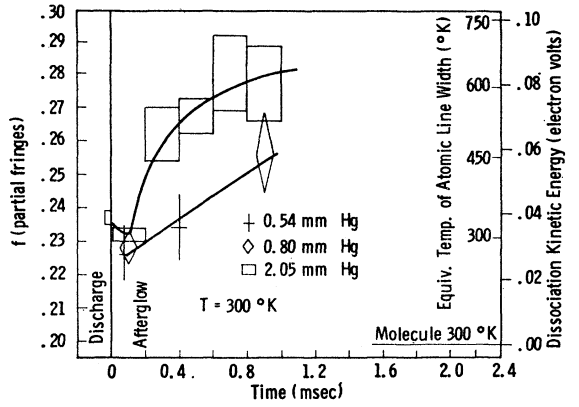

FIG. 8. Variation of the observed linewidths with time during the discharge and in the afterglow of helium at 300°K. The widths are expressed as fractions f of the free spectral range of the etalon. The scales at the right refer, respectively, to the equivalent atom temperature required to yield the observed width and to the dissociation kinetic energy E_D which must be added to the initial molecular ion thermal motion to give the observed width.

pressures at $T=300$°K in Fig. 8 and at $T=77$°K in Fig. 9. Here, improved Fabry-Perot plates were used. They had dielectric reflecting coatings of higher reflectivity and lower absorptivity than the silver films used on the previous plates. Thus, the instrumental broadening was reduced relative to Fig. 7. The horizontal widths of the symbols indicate the time gate during which the photomultiplier was made sensitive to light; the vertical extent of the symbols indicates the uncertainty in the linewidth determinations in these low-signal measurements.

From the temperature scale at the right of the figure, it will be seen that, as noted previously at 300°K, the line during the discharge at 77°K shows broadening in excess of ambient temperature effects, consistent with atom recoil at impact of the exciting electrons. Immediately afterwards, in the early afterglow at 300°K and at 77°K, the linewidths decrease to values indistinguishable from the widths appropriate to the ambient temperatures. This observation is consistent with the proposed mechanism for production of the early afterglow radiation by electron impact on metastable atoms, since the ~3 eV electron energy required to excite to the radiating $3\,^3D$ state causes negligible recoil in the struck atom compared to its thermal speed.

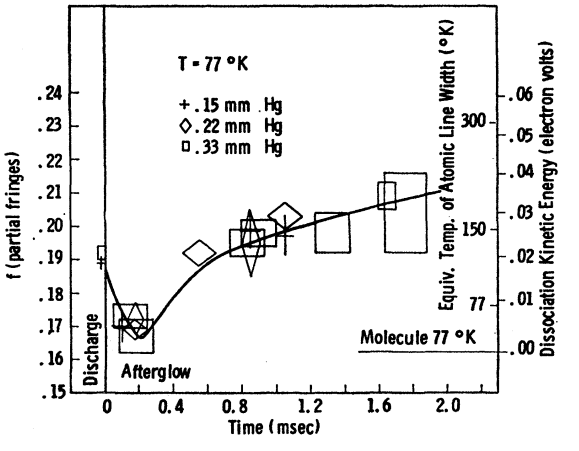

FIG. 9. Variation of the observed linewidths in helium at 77°K.

It will be seen in both Figs. 8 and 9 that the observed linewidths increase with time in the later afterglow. These observations are consistent with the expectation that, as the contribution to the radiation by metastable atom excitation decreases and that due to dissociative recombination increases, the line should increase in width, until a maximum width is attained when recombination alone is important. Unfortunately, the decrease in intensity with time in the afterglow does not permit line width measurements to be carried beyond ~1 msec at 300°K and ~2 msec at 77°K.

Although a pronounced line broadening is detected in the late afterglow, if one calculates the dissociation kinetic energy required to yield the observed width,[24] then, as the second scale at the right of the figures ndicates, the inferred change of potential energy between the initial and final states of reaction (13) is rather smaller than one would estimate. As mentioned in Sec. III C.3, it is difficult to assure radiation of the excited, fast moving atom before slowing down by elastic collisions or excitation transfer to slow atoms takes place. If one argues that the momentum transfer cross section for scattering of $3\,^3D$ atoms by normal helium atoms is the same magnitude as for the metastable $2\,^3S$ atoms, namely, $Q_m=8\times10^{-15}$ cm^2,[18,19] then the excess energy of the atoms produced by dissociative recombination decays at the rate $\nu_{\text{coll}}\sim10^8$ sec^{-1} at 2 mm Hg pressure. Alternatively, if the excitation transfer cross section is of the same order of magnitude ($\sim10^{-14}$ cm^2) as the momentum transfer cross section, appreciable "narrowing" of the observed line will also occur by the transfer process. Excitation transfer cross sections, even for nonresonant cases, attain large values. For example, Gabriel and Heddle[25] deduce values of $Q_{\text{transfer}}\gg10^{-15}$ cm^2 for various $n\,^1P\rightarrow n\,^1D$ transfers ($n=3, 4, 5, 6$) at thermal energy. Thus, it is quite possible that in these studies we have been able to observe only a small fraction of the initial dissociation kinetic energy produced by the recombination process.

A final point, mentioned briefly in an earlier paper,[3] involves accounting for the appearance of such radiation as λ5876 and λ4472 as strong afterglow lines resulting from dissociative recombination. As will be seen from Fig. 10, with an expected binding energy of ~2 eV for (He_2^+),[26] it is necessary to postulate that the molecular

[24] It is assumed that the molecular ions have a speed determined by the ambient temperature. Then, since the dissociation energy is shared equally by the two helium atoms, one may calculate the line broadening to be expected for various values of the dissociation kinetic energy.

[25] A. H. Gabriel and D. W. O. Heddle, Proc. Roy. Soc. (London) **A258**, 124 (1960).

[26] E. A. Mason and J. T. Vanderslice, J. Chem. Phys. **29**, 361 (1958).

ions are in vibrationally excited states as they undergo dissociative recombination in order to produce the high-lying atomic states which yield the observed lines. (The figure is schematic, the vibration levels having been calculated for a Morse potential function.) The formation of the molecular ions in high-lying vibration states is a reasonable consequence of the assumed conversion reaction (12), in which the most likely binding collision is one in which a minimum loss of kinetic energy between two atoms takes place. Recent studies of vibration persistence in gases[27] have indicated that, for such well-separated vibration levels as in He_2^+, the probability of de-excitation by transfer of vibration energy to kinetic energy of relative motion at a collision with a helium atom is likely to be very small, $<10^{-8}$. Thus, on the millisecond time scale of our measurements, the ions should persist in the higher vibration states for an appreciable fraction of the observing interval.

In summary, the initial goal of determining whether or not the dissociative process is responsible for the large electron-ion recombination losses observed in microwave afterglows has not been fully achieved. The observations are consistent with a model of the helium afterglow in which, at later times, recombination becomes an important source of the afterglow radiation. At these times the emitted lines definitely show broadening in excess of thermal width. If one were to argue that the late afterglow broadening is the result of some process other than dissociative recombination, then one is faced with the dilemma of explaining how the excited atom temperature in the early afterglow sinks to thermal values and then increases rather abruptly. Clearly, such effects as pressure broadening cannot explain these observations, and careful monitoring of molecular band

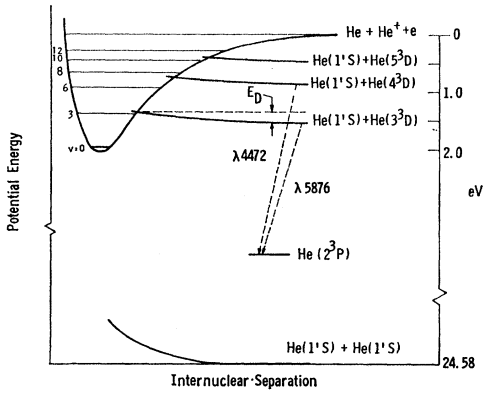

FIG. 10. Schematic representation of the potential curves required to explain the observations of strong λ4472 and λ5876 afterglow lines in terms of dissociative recombination. It will be seen that long-lived vibrationally excited states of the molecular ion are involved.

radiation intensities indicates that such spurious broadening effects do not account for the observed increase in width. Thus, dissociative recombination appears the most likely source of the modestly increased linewidths in the late afterglow. Studies of line shapes in neon afterglows, where recombination is the predominant electron removal process over a wider range of experimental variables, are in progress.[28]

ACKNOWLEDGMENTS

The authors wish to thank the members of the Atomic Physics Group, especially L. S. Frost and A. V. Phelps, for their interest and helpful discussions of this problem.

[27] S. J. Lukasik and J. E. Young, J. Chem. Phys. **27**, 1149 (1957).

[28] T. R. Connor and M. A. Biondi, Sixteenth Gaseous Electronics Conference, Pittsburgh, Pa., October, 1963 (unpublished); Bull. Am. Phys. Soc. **9**, 184 (1964).